AJNR

A CT Method to Measure Hemodynamics in Brain Tumors: Validation and Application of Cerebral Blood Flow Maps

Aleksa Cenic, Darius G. Nabavi, Rosemary A. Craen, Adrian W. Gelb and Ting-Yim Lee

AJNR Am J Neuroradiol 2000, 21 (3) 462-470
http://www.ajnr.org/content/21/3/462

AJNR Am J Neuroradiol 21:462–470, March 2000

A CT Method to Measure Hemodynamics in Brain Tumors: Validation and Application of Cerebral Blood Flow Maps

Aleksa Cenic, Darius G. Nabavi, Rosemary A. Craen, Adrian W. Gelb, and Ting-Yim Lee

BACKGROUND AND PURPOSE: **CT is an imaging technique that is routinely used for evaluating brain tumors. Nonetheless, imaging often cannot show the distinction between radiation necrosis and neoplastic growth among patients with recurrent symptoms after radiation therapy. In such cases, a diagnostic tool that provides perfusion measurements with high anatomic detail would show the separation between necrotic areas, which are characterized by low perfusion, from neoplastic areas, which are characterized by elevated CBF. We attempted to validate a dynamic contrast-enhanced CT method for the measurement of regional CBF in brain tumors, and to apply this method by creating CBF maps.**

METHODS: **We studied nine New Zealand White rabbits with implanted brain tumors. We obtained dynamic CT measurements of CBF, cerebral blood volume (CBV), and permeability surface (PS) from the tumor, peritumor, and contralateral normal tissue regions. In all nine rabbits (two studies per rabbit), we compared CT-derived CBF values with those simultaneously obtained by the standard of reference ex vivo microsphere technique. Using CT, we examined three rabbits to assess the variability of repeated CBF and CBV measurements; we examined the other six to evaluate regional CBF reactivity to arterial carbon dioxide tensions. Finally, CT CBF maps were obtained from a rabbit with a brain tumor during normocapnia and hypocapnia.**

RESULTS: **We found a significant linear correlation ($r = 0.847$) between the regional CT- and microsphere-derived CBF values, with a slope not significantly different from unity (0.99 ± 0.03, $P > .01$). The mean difference between regional CBF measurements obtained using both methods did not significantly deviate from zero ($P > .10$). During normocapnia, tumor had significantly higher CBF, CBV, and PS values ($P < .05$) than did peritumor and normal tissues. The variability in CT-derived CBF and CBV measurements in the repeated studies was 13% and 7%, respectively. CT revealed no significantly different CBF CO_2 reactivity from that determined by the microsphere method ($P > .10$). The CBF map of tumor regions during normocapnia showed much higher flow than normal regions manifested, and this difference was reduced on the hypocapnia CBF map.**

CONCLUSION: **The dynamic CT method presented herein provides absolute CBF measurements in brain tumors that are accurate and precise. Preliminary CBF maps derived with this method demonstrate their potential for depicting areas of different blood flow within tumors and surrounding tissue, indicating its possible use in the clinical setting.**

CT and MR imaging techniques are used routinely for evaluating brain tumors (1). These diagnostic tools provide important morphologic information regarding location, size, and mass effect of brain tumors. With the administration of contrast agents, these imaging techniques can more accurately demarcate the boundaries of neoplastic tissue from surrounding normal tissue as well as provide data on the presence and extent of vasogenic edema arising from an impaired blood-brain barrier (BBB) (1). Among patients with recurrent symptoms after radiation therapy, however, the neuroradiologist may confront problems with differentiating between radiation necrosis and recurrent neoplastic growth (2–5). In such cases, a diagnostic tool that provides perfusion measurements with high anatomic detail could delineate the boundaries of ne-

Received March 4, 1999; accepted after revision August 24, 1999.

From the Imaging Research Laboratories (A.C., D.G.N., T-Y.L.), John P. Robarts Research Institute, London; Medical Biophysics Department (A.C., T-Y.L.), The University of Western Ontario, London; Imaging Division, Lawson Research Institute (A.C., T-Y.L.), St. Joseph's Health Centre, London; and Anesthesia Department (R.A.C., A.W.G.), London Health Sciences Centre, London, Ontario, Canada.

Presented in part at: the XIXth International Symposium on Cererbral Blood Flow, Metabolism and Function; 1999: Copenhagen, Denmark.

Address reprint requests to Ting-Yim Lee, PhD, Imaging Research Laboratories, John P. Robarts Research Institute, P.O. Box 5015, 100 Perth Drive, London, Ontario, N6A 5K8 Canada.

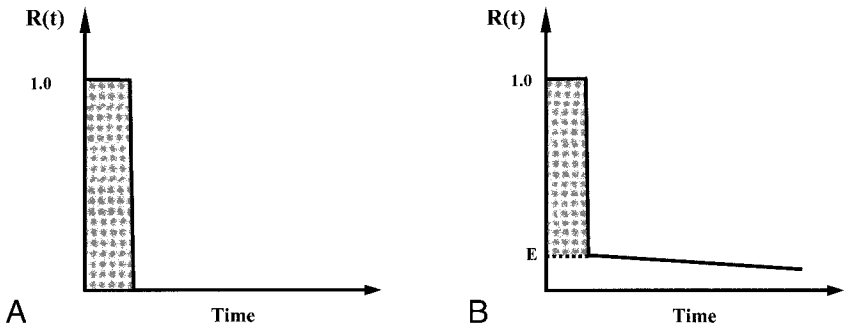

FIG 1. *A,* Schematic representation of IRF in a tissue with an intact (ie, impermeable to contrast molecules) BBB.

B, Schematic representation of an IRF, R(t), in tissue with a permeable BBB. The first plateau reflects the intravascular phase of the contrast material. The second (and much lower) plateau reflects the extravascular phase. The extraction fraction, E, is derived by dividing the second plateau height by the first plateau height.

crotic areas, which are characterized by low perfusion, thus distinguishing them from neoplastic tissue with elevated cerebral blood flow (CBF). Moreover, CBF measurements would not only provide important information regarding treatment outcomes, but also would allow one to investigate the hemodynamic effects of the lesion on surrounding tissue. Such an imaging tool could supplement the morphologic information obtained from CT or MR with functional information related to tissue-specific perfusion, increasing the accuracy of brain tumor diagnosis.

Currently, positron emission tomography (PET) is the standard of reference in providing in vivo functional information concerning perfusion and metabolism of patients with neurologic disease (1). During the last decade, several investigators have reported on the use of PET for differentiating neoplastic from normal tissue through analysis of CBF, cerebral blood volume (CBV), BBB permeability, and metabolism (6–10). With the wider clinical availability of single-photon emission CT (SPECT) and MR scanners, various investigators have proposed using these techniques to replace PET studies in the evaluation of cerebral hemodynamics (eg, CBF and CBV) in brain tumor patients. These studies have shown promise in differentiating radiation necrosis from recurrent tumor growth and providing some insight regarding tumor grade (11–15).

The routine use of CT for initial neuroradiologic diagnosis, as well as its widespread clinical availability, prompted our group to develop a contrast-enhanced, dynamic CT method that can provide absolute measurements of regional CBF and CBV in normal tissue with an intact BBB (16). In tumors and other neurologic disorders (eg, inflammation, chronic ischemia), however, the BBB is impaired, leading to extravasation of contrast material into the extravascular space (EVS) from the intravascular space (IVS). In such cases, the commonly used method of dividing the area beneath the tissue enhancement curves by the arterial enhancement curve leads to an overestimation of CBV (17, 18). Because our original method (16) employs this approach in the calculation of CBV, the subsequent application of the Central Volume Principle (19) would also result in CBF being overestimated. In order to apply our dynamic CT method in tissue with a permeable BBB (eg, tumor), leakage of contrast material across the BBB must be accounted for in the calculation of CBV and CBF.

We describe a theoretical approach that extends the ability of our deconvolution method to provide absolute CBV and CBF measurements in tissue with a permeable BBB. The extension also enables the simultaneous measurement of the capillary permeability surface area product (PS) with CBV and CBF. The purpose of this study was twofold. First, we attempted to validate the accuracy of our regional CT-derived CBF measurements against the standard of reference ex vivo microsphere technique in experimental brain tumors. Second, we sought to apply our method by developing absolute CBF maps and demonstrating their application in rabbits with brain tumors. We expect that clinical trials will be able to apply the developed techniques described herein as easily as in this current experimental study.

Theory

As previously described (16), the Central Volume Principle as derived by Meier and Zierler (19) describes the relationship between CBF, CBV and MTT with Equation 1:

$$\text{CBF} = \frac{\text{CBV}}{\text{MTT}} \quad (1)$$

CBF is the flow (mL/min/100 g) through a given vascular network in the brain. CBV is the volume of blood (mL/100 g) within the vessels. MTT is the mean transit time of all blood elements entering at the arterial input and leaving at the venous output of the vascular network.

Axel (17) and Cenic et al (16) described a CT-derived Impulse Residue Function (IRF), which measures a unit of contrast material injected as a bolus at an arterial input and the mass of contrast media remaining in the given vascular network over time. A schematic representation of an IRF for the case of an intact BBB is shown in Figure 1A. The plateau width corresponds to the minimum transit time of the contrast material flowing through the vascular network (ie, interval during which the total volume of injected contrast material remains within the vessels). After this finite duration, con-

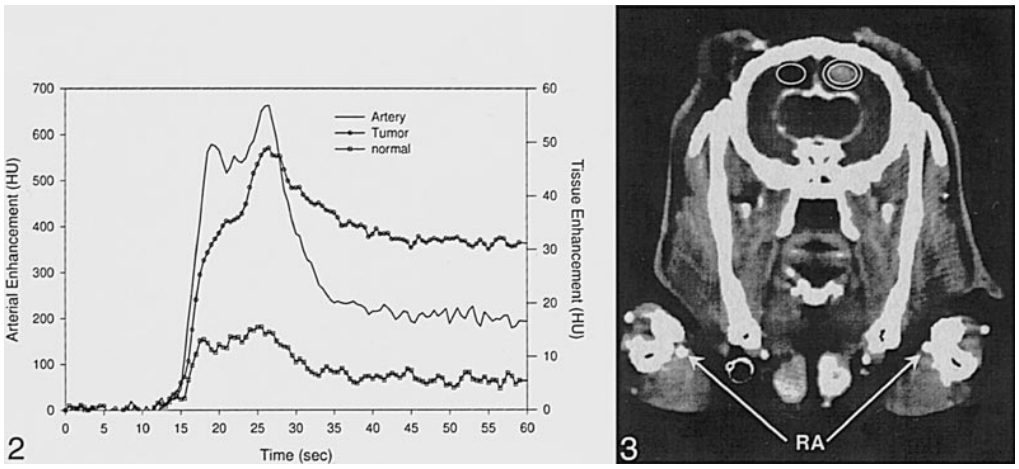

FIG 2. Examples of dynamic CT-measured contrast-enhancement curves of an artery (*line*), normal tissue (*squares*), and tumor (circles) in a rabbit with brain tumor. For clarity, the tissue curves are displayed using a different scale of CT numbers (*right axis*). Thus, the arterial enhancement curve (*left axis*) is more than 10 times higher than that of the tumor curve, and 50 times higher than that of the normal tissue curve. Note the higher washout phase of the tumor curve relative to the normal tissue.

FIG 3. Contrast-enhanced CT image illustrating tumor, peritumor and contralateral normal ROIs found in a rabbit. The radial arteries (RA) are clearly displayed at the bottom of the figure (adjacent to the radial and ulna bones).

trast material begins to leave the vascular network, leading to the drop of the IRF to zero. For normal cerebral tissue with an intact BBB, the MTT is calculated from the IRF, R(t), by the area-over-height formula (16).

For cases in which the BBB is defective (eg, tumor), however, injection of contrast material will result in diffusion of contrast molecules from the IVS into the EVS. The paths followed by contrast molecules through the vascular network can be classified as those that remain entirely intravascular and those that leak into the EVS and then diffuse again into the IVS (20). Let $R_i(t)$ denote the IRF for those contrast molecules that remain in the IVS during their *entire* transit through the vascular network, and let $R_e(t)$ denote the IRF for contrast molecules that leak across the BBB into the EVS at *some time* during their transit through the vascular network. If E is the extraction fraction (ie, the fraction of contrast material that leaks into the EVS from the IVS), then the IRF for a brain region with a permeable BBB is given by Equation 2:

$$(2) \qquad R(t) = E \cdot R_e(t) + (1 - E) \cdot R_i(t)$$

Note that, by definition, both $R_i(0)$ and $R_e(0)$ should be equal to 1.0 (21). Figure 1B shows a schematic representation of Equation 2. The second plateau, which is lower in height but much longer in duration than the first plateau, occurs because of the slow diffusion of contrast material back into the IVS from the larger EVS volume (20). This fraction in the EVS remains visible to the CT scanner until it is completely cleared by diffusion back into the IVS and then cleared from the vascular network by the CBF. As shown in Figure 1B, the initial point of the second plateau of R(t) represents the EVS fraction (ie, E = {2nd plateau height of R(t)}/{1st plateau height of R(t)}). Furthermore, by extrapolating the initial EVS plateau to time zero and subtracting it from R(t), $(1\text{-}E)R_i(t)$ is obtained.

As discussed previously (16), the direct experimental measurement of R(t) cannot be obtained from patients because this requires the invasive injection of contrast material into an input artery. For clinical applications, an alternative strategy is to infuse contrast material intravenously over a very short duration and then measuring contrast enhancement over time for a brain region, Q(t), with CT scanning. As shown by Meier and Zierler (19), Q(t) is expressed by Equation 3:

$$(3) \qquad Q(t) = CBF.C_a(t) * R(t)$$

$C_a(t)$ is the enhancement curve measured at the arterial input, R(t) is the IRF for the given brain region (with an intact or impaired BBB), and * denotes the convolution operator. With the increased spatial and temporal resolution of current CT scanners, Q(t) and $C_a(t)$ can be accurately measured after a rapid intravenous injection of contrast material (Fig 2). Assuming that the arterial enhancement curve measured at a peripheral artery (eg, ear or radial) represents the arterial input to the brain region, then from Equation 3, *deconvolution* of the CT-measured Q(t) and $C_a(t)$ curves provides an estimate of CBF.R(t)—ie, R(t) scaled by CBF, or $R^s(t)$—for the brain region (16). With $R^s(t)$ known, E can be calculated by the ratio of the heights of the first and second plateau, as discussed before. Back extrapolation of $R^s(t)$ and subtraction of the extrapolated result will give an estimated CBF.$(1\text{-}E).R_i(t)$ or the scaled IVS IRF, $R_i^s(t)$.

Because $R_i(t)$ is the IRF for the contrast molecules that stay within the IVS during their entire transit through the vascular network, MTT, as in the case of an intact BBB, can be expressed in Equation 4:

$$(4) \qquad MTT = \frac{\int_0^\infty R_i^s(t)\,dt}{R_i^s(0)}$$

$R_i^s(0)$ is the plateau (or maximum) height of $R_i^s(t)$. Also, because $R_i^s(t)$ is the product of CBF and $R_i(t)$ and $R_i(0)$ is unity, we have Equation 5:

$$(5) \qquad CBF = \frac{R_i^s(0)}{(1 - E)}$$

Equation 6 follows from Equations 4 and 5:

$$(6) \qquad CBV = \frac{\int_0^\infty R_i^s(t)\,dt}{(1 - E)}$$

Renkin (22) and Crone (23) expressed E in Equation 7:

$$(7) \qquad E = 1 - e^{-(PS/CBF)}$$

PS (mL/min/g) is the permeability surface area product of the BBB to contrast material. From Equation 7, if both CBF and E are known, then Equation 8 follows:

$$(8) \qquad PS = -CBF.\ln(1 - E)$$

Methods

Study Protocol

We used nine male New Zealand White rabbits in experiments approved by the Animal Ethics Committee at the University of Western Ontario (London, Ontario, Canada). We harvested VX2 carcinoma cells from a 3- to 4-cm-diameter tumor in one of the hind legs of a host rabbit that had been injected with the same cell line 2–3 weeks prior. Approximately 5×10^5 cells were injected into the right parietal lobe (3 mm below the dura mater) of a study rabbit through a small burr hole. The tumor was then allowed to grow for at least 7 days. From day 7 onward, we performed a contrast-enhanced coronal CT scan of the brain every other day to determine the tumor size. When the tumor reached approximately 0.4 cm in diameter (as viewed on the coronal CT image), we performed the experimental study on the following day by using the protocol described herein.

On the day of the experiment, we surgically prepared each rabbit that had been implanted with a brain tumor, as described in our previous CT CBF validation study in normal rabbits (16). During the experiment, anesthesia was maintained with 1.5% isoflurane. Mean arterial blood pressure was continuously monitored, and rectal temperature was maintained at approximately 38.5°C with a recirculating water pad and heat lamp. Hematocrit was measured every 30 minutes to ensure that the blood volume was not rapidly decreasing from withdrawal of blood samples for blood gas determination and microsphere-derived CBF measurements. Because arterial carbon dioxide tension ($PaCO_2$) measurements were not obtained during each microsphere study and CT CBF study, the average of the $PaCO_2$ values immediately before and after each study was considered to be the $PaCO_2$ value for both CBF measurements.

We measured regional microsphere CBF in all nine rabbits to evaluate the accuracy of our CT method of measuring CBF under various physiologic conditions. We studied six of nine rabbits to evaluate the sensitivity of our CT method of measuring CBF for detecting cerebrovascular responses to decreasing arterial $PaCO_2$ levels. In these CBF CO_2 reactivity experiments, the CT- and microsphere-derived measurements were first obtained during normocapnia ($PaCO_2 \approx 40$ mm Hg), and then during hypocapnia ($PaCO_2 \approx 25$ mm Hg), with at least a 30-minute wait between the normocapnia and hypocapnia measurements. This time delay allowed for the clearance of contrast material from the circulation. We induced hypocapnia by increasing the ventilation rate of the rabbit. We studied the remaining three rabbits to evaluate the precision of our dynamic CT measurements. In these precision experiments, repeated CBV and CBF measurements were made in the tumor, peritumor, and contralateral normal tissue regions during two normocapnic studies, with the same 30-minute delay as in the experiments involving hyperventilation.

Dynamic CT Scanning Protocol

After anesthesia was induced, the animal was placed in the prone position on the patient couch with its head and forelimbs secured in the head holder supplied with the CT scanner. Precontrast 3×3-mm coronal scans were prescribed from a lateral scout image. The brain tumor was located using these precontrast coronal scans. Upon intravenous injection of 1 mL Ultravist 300 (Berlex, Canada), we then performed 1-mm-spacing coronal scanning of the same (3-mm) thickness, covering the entire tumor, in order to locate the coronal section with the largest tumor cross section. This section was then chosen as the study slice for the two sequential dynamic CT studies.

The dynamic (cine) CT imaging (continuous scanning without interscan delay at the same level) parameters were as follows: 80 kVp, 80 mA, 512 matrix, 10-cm field of view, 3-mm slice thickness, and 1 s/scan. In the reconstruction of CT images, a back-projection filter with a cut-off frequency of 10 line pairs per cm was employed. Dynamic scanning was initiated 5 seconds before a bolus of contrast material (1.5 mL Ultravist/300 kg body weight) was infused into an ear vein at a rate of 0.3 mL/s by using an automated injector (Medrad Injector, Medrad, PA). This delay in contrast material injection allowed for the acquisition of precontrast baseline images (ie, background data for image analysis). Dynamic scanning was maintained during the bolus injection of contrast material and continued for the remaining minute.

Ex Vivo CBF Microsphere Measurements

We obtained regional CBF measurements by using fluorescent-labeled (or radioisotope-labeled) microspheres in a manner similar to that described in our previous article (16). CBF was first measured using the microsphere method, and then immediately afterward by the dynamic CT method. The close spacing in time (< 2 min) ensured that similar hemodynamic conditions existed during performance of both CBF measurement techniques. Upon completion of the experiment, tissue samples from each cerebral hemisphere at the level of the brain tumor corresponding to the CT tissue regions (Fig 3) were trimmed accordingly.

CT Data Analysis

Regions of interest (ROIs) in the CT brain images were drawn in the tumor, peritumor, and contralateral normal regions (Fig 3) by using the following procedure. First, an ROI was drawn incorporating the entire tumor—the most enhanced area of the right hemisphere—as shown in Figure 3. This tumor ROI was then reflected about the midline into the left cerebral hemisphere to create the contralateral normal ROI. Finally, we

created the peritumor ROI by expanding the tumor ROI by 5 to 6 pixels. These ROIs were drawn such that no major blood vessels were present within the regions. Q(t) for each tissue ROI was then obtained by subtracting the regional mean CT-derived number obtained in precontrast images from the mean CT-derived number obtained in sequential contrast-enhanced images.

The arterial contrast concentration curve, Ca(t), was obtained from one of the radial arteries (Fig 3) or from an ear artery, as previously described (16). As in the case of Q(t), $C_a(t)$ was also determined by subtracting the mean CT-derived number in the vessel ROI obtained by precontrast scanning from the mean CT-derived number obtained by contrast-enhanced scanning. The measured $C_a(t)$ was then corrected for partial volume averaging (16).

Correction for Difference in Tissue and Large-Vessel Hematocrit

Contrast material is confined to the plasma phase of blood. Provided that the hematocrit of blood remains the same in peripheral (large) blood vessels and tissue capillaries, the enhancement measured in tissue and blood will be equivalent. To correct tissue enhancement for the difference in large-vessel and small-vessel (tissue) hematocrit, Q(t) has to be multiplied by the factor $\varphi = (1\text{-H})/(1\text{-rH})$ where H is the hematocrit of blood in large vessels and r (0.8) is the ratio of small-to-large vessel hematocrit for small animals (24).

CBF Maps

The brain tissue enhancement was assessed in approximately 1000 3 × 3 pixel blocks covering the entire brain. Using the measured arterial input curve with the respective tissue curve for each pixel block, our deconvolution algorithm (16) was used to generate a CBF map by determining its value in each pixel block. CBF maps were determined for a single rabbit (randomly chosen from the six rabbits in which hyperventilation was induced) both during normocapnia and hypocapnia. The change in CBF from hyperventilation was evaluated by comparing the mean CBF over the entire cerebral map for both studies and by subtracting the hypocapnia map from the normocapnia map to observe changes in CBF from hyperventilation.

Statistical Analysis of Data

Statistical analysis was performed using SPSS 9.0 Scientific Software Packages (Chicago, IL). Standard descriptive statistics, such as mean ±SD, were calculated. Two-tailed *t*-tests (paired or unpaired) were used to determine the statistical significance of changes in normally distributed data. Pearson product moment correlation was used to determine the correlation between microsphere and CT measurements for both regional CBF values and absolute CBF CO_2 reactivity. Linear regression analysis was used to determine the slope of the correlation plot between the microsphere- and CT-derived measures of CBF. A one-sample *t*-test (two-tailed) was used to test the mean of the distribution of differences between microsphere- and CT-derived CBF values against zero. An analysis of variance (ANOVA) for repeated measures was used to determine the percent variability of our CT CBF and CBV measurements as well as that of the microsphere CBF measurements. Statistical significance was declared at the $P < .05$ level.

Results

Table 1 details the controlled and monitored physiologic parameters for the six rabbits in which hyperventilation was induced and the three rabbits used in precision studies. A paired *t*-test revealed no significant change in the physiologic parameters over the duration of the two sequential studies ($P > .10$), except in the mean $PaCO_2$ values for the studies involving hyperventilation. The mean change in $PaCO_2$ (±SD) caused by hyperventilation was 14.0 ± 1.9 mm Hg ($P < .01$).

TABLE 1: Controlled and monitored physiologic parameters

	Study 1	Study 2
Hyperventilation Studies (n = 6)		
$PaCO_2$ (mm Hg)	38.8 ± 0.9	24.8 ± 1.3*
MABP (mm Hg)	79.7 ± 8.3	79.5 ± 7.0
Temperature (°C)	38.7 ± 0.3	38.6 ± 0.3
Hematocrit	34.0 ± 1.1	32.8 ± 2.5
Precision Studies (n = 3)		
$PaCO_2$ (mm Hg)	41.3 ± 1.1	37.5 ± 3.3
MABP (mm Hg)	80.7 ± 7.4	78.7 ± 2.1
Temperature (°C)	38.6 ± 1.0	38.7 ± 1.0
Hematocrit	34.3 ± 2.5	32.5 ± 2.2

Note.—Values are Mean ± SD; the mean (n = 9) rabbit mass was 3.1 ± 0.4 kg.

* $P < .01$ versus Study 1 as determined by paired *t*-test.

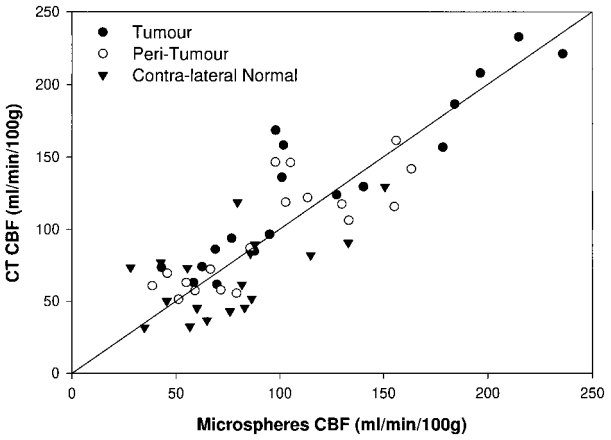

FIG 4. Dynamic CT measurements plotted against microsphere measurements of regional CBF (mL/min/100 g) for 54 ROIs (18 ROIs for each tumor, peritumor, and normal tissue) in nine rabbits with brain tumor. A strong correlation was found between these two sets of measurements ($r = 0.847$). The slope of the regression line (0.99 ± 0.03, $P < .001$) was not significantly different from unity.

A comparison of regional CBF values in tumor, peritumor, and contralateral normal tissue was determined using both the microsphere and dynamic CT methods and revealed a significant positive correlation between the two methods ($r = 0.847$) (Fig 4). As shown by the near-unity slope in Figure 4 (m = 0.99 ± 0.03), the dynamic CT–derived CBF values in both normal and neoplastic tissue compared well with those obtained using the standard of reference microsphere method. The mean difference between microsphere- and CT-derived CBF values for all of the 54 regions was not statistically significant (-1.8 ± 25.9 mL/min/100 g, $P > .10$). Linear regression analysis between microsphere-

TABLE 2: Comparison of mean regional CBF changes (ΔCBF) to decreased CO_2 levels using both the microsphere and the dynamic CT methods in six rabbits

Tissue ROI	CO_2 Reactivity (ΔCBF/mm Hg)		*t*-test *P*-value	*t*-test power
	Microspheres	*Dynamic CT*		
Tumor	3.42 ± 4.66	4.27 ± 4.48	0.75	0.76
Peritumor	1.84 ± 3.25	2.64 ± 2.88	0.66	0.69
Normal tissue	1.13 ± 2.22	0.88 ± 1.84	0.83	0.84

Note.—CO_2 reactivity in mL/min/100g per mm Hg; values are Mean ± SD.

TABLE 3: Comparison of mean regional CBF, CBV, and PS values as determined by dynamic CT in 12 normocapnia rabbit studies

ROI	CBF (mL/min/100 g)	CBV (mL/100 g)	PS (mL/min/100 g)
Tumor	150.4 ± 56.3*	5.62 ± 1.03*	4.52 ± 2.60*
Peritumor	106.6 ± 39.4†	3.15 ± 0.85†	1.07 ± 0.85†
Normal	77.1 ± 27.7	1.95 ± 0.26	0.23 ± 0.30

* $P < 0.05$ versus values in peritumor and normal regions as determined by *t*-test (two-tailed). Values are Mean ± SD.

† $P < 0.05$ versus values in normal region as determined by *t*-test (two-tailed). Values are Mean ± SD.

and CT-derived CBF measurements for tumor, peritumor, and contralateral normal tissue types revealed slopes of 1.05 ± 0.05, 0.99 ± 0.05, and 0.83 ± 0.07, respectively, and correlation coefficients of 0.886, 0.784, and 0.458, respectively. The mean difference between the two CBF measurement methods was not significantly significant for each tissue type (tumor [$P > .05$]), peritumor [$P > .10$], and contralateral normal [$P > .10$]).

Table 2 compares the dynamic CT measurements of regional CBF CO_2 reactivity upon hyperventilation (ie, change of CBF from normocapnia to hypocapnia) to those obtained by the microsphere method in tumor, peritumor, and normal tissue. A *t*-test revealed no significant difference ($P > .10$, Power 0.7 to 0.8) between CT and microsphere findings of regional CBF CO_2 reactivity.

Regional CBF, CBV, and PS were obtained using the dynamic CT method during normocapnia for 12 rabbit studies (six from the hyperventilation studies, and six from the precision studies). The mean regional values are shown in Table 3. Using the *t*-test, regional CBF, CBV, and PS measurements were all significantly higher ($P < .05$) in the tumor than in the peritumor region, and values in the peritumor region were also significantly larger ($P < .05$) than in the contralateral normal tissue. On average, tumor vessels were about 20 times more permeable than were those in the contralateral normal hemisphere.

The reproducibility of the microsphere and dynamic CT methods for measuring regional CBF during steady-state normocapnia was evaluated using an ANOVA for repeated measures in three rabbits (two sequential studies per rabbit). CBF measurements for all three regions (tumor, peritumor, and normal tissue) were used in this analysis. The variability in CBF measurements was 26.2% with the microsphere method and 13.2% for the dynamic CT method. Moreover, the mean difference between CBF measurements obtained using either the dynamic CT or microsphere method for sequential studies was not statistically significant ($P = .67$ [microsphere]; $P = .77$ [dynamic CT]). The variability of repeated CT-derived CBV measurements was 7.3%, which was similar to CBF measurements. The mean difference between CT-derived CBV measurements for sequential studies was not statistically significant ($P = .95$).

A comparison of the CBF maps in a rabbit with an implanted tumor in the right hemisphere (Fig 5A), first during normocapnia (Fig 5B) and then during hypocapnia (Fig 5C), revealed a 27% global reduction in CBF in the latter study. The mean CBF values within the entire maps for the normocapnia and hypocapnia studies were 66.6 and 48.7 mL/min/100 g, respectively. An overall reduction in CBF upon hyperventilation is clearly seen in the subtraction map (normocapnia—hypocapnia) of Figure 5D. The mean global CBF CO_2 reactivity was approximately 1.3 mL/min/100 g per mm Hg. As shown from the individual maps, the tumor was clearly distinguishable from the low-flow normal tissue regions.

Discussion

The clinical benefit of a diagnostic tool that simultaneously provides both anatomic and functional information prompted us to extend our previously described dynamic CT method (16), which is only applicable to normal tissue, to the simultaneous measurements of CBF, CBV, and PS in brain tumors. In the current studies, we sought to assess the accuracy and precision of our method in measuring CBF, CBV, and PS in discrete tissue regions with a permeable BBB (eg, tumors), and then to apply our validated CT CBF method to create functional maps in a rabbit brain tumor model. The VX2 carcinoma tumor model was selected because it has characteristics similar to human metastatic brain tumors (25). Also, it has the advantages of a high rate of successful implantation, a short induction time, good reproducibility, and stable histologic characteristics (26).

In the first part of this study, we assessed the accuracy of our CT-derived CBF measurements by comparing them against simultaneous microsphere-derived CBF measurements in tumor, peritumor, and normal tissue. A very good correlation ($r = 0.847$) was found between the dynamic CT and the microsphere CBF findings (Fig 4). This correlation is very similar to that of our previous results in normal rabbits ($r = 0.837$) (16) and is also comparable to that of xenon CT–derived CBF mea-

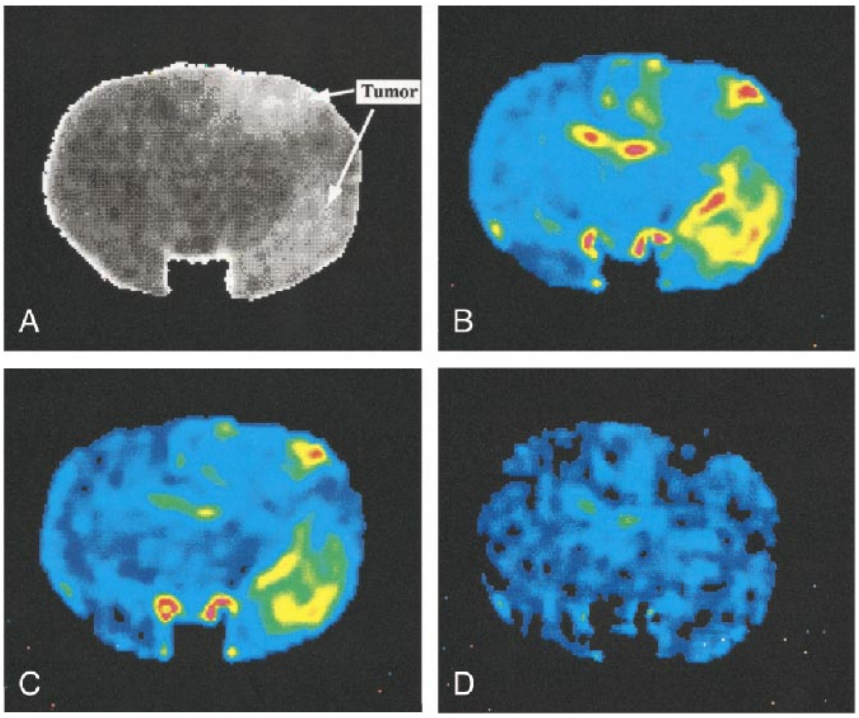

FIG 5. CBF maps derived from a rabbit with brain tumor. The CBF values, ranging from low-to-high flow are color-coded from black (0 mL/min/100 g) to blue and green (100 mL/min/100 g) to yellow and red (200 mL/min/100 g). For both $PaCO_2$ levels, the tumor is clearly delineated by the red and yellow colors.

A, Plain (precontrast) CT Image. The following X-ray CT parameters were used to acquire the image: 80 kVp, 80 mA, 10-cm field of view, and 3-mm slice thickness. Hyperdense areas corresponding to the tumor were observed in the right parietal and temporal regions.

B, Normocapnia CBF map. CBF in the tumor ranged from 66 to 208 mL/min/100 g, whereas CBF in the contralateral normal hemisphere ranged from 14 to 75 mL/min/100 g.

C, Hypocapnia CBF map. The maximum and minimum CBF values in tumor were 56 and 170 mL/min/100 g, whereas the contralateral normal hemisphere showed CBF values ranging from 3 to 43 mL/min/100 g.

D, Subtraction of the hypocapnia CBF map from the normocapnia map. The mean global CBF difference was 18.7 mL/min/100 g. Reduction in CBF upon hyperventilation is shown in both tumor and normal tissues. The green circular areas in the center of the brain are cerebral arteries.

surements in normal baboons ($r = 0.69$ for normocapnia, $r = 0.83$ for hypocapnia studies) (27). Because the regression slope of CT versus microsphere CBF measurements was near unity ($m = 0.99 \pm 0.03$, $P > .05$) and the mean differences between *all* regional microspheres and CT CBF values were not significantly different from zero ($P > .10$), a good agreement was demonstrated between both methods. Nonetheless, comparing the CBF regression slopes (CT versus microspheres) for the different tissue regions showed that those for the tumor and peritumor regions did not significantly deviate from unity, whereas the contralateral normal slope ($m = 0.83 \pm 0.07$) had a significant deviation from unity ($P < .05$). This underestimation of CBF values in normal tissue by dynamic CT was not observed in our previous study in normal rabbits (16), where the slope was not significantly different from unity ($m = 0.97 \pm 0.03$, $P > .05$). The observed significant deviation of the correlation slope from unity in the present study may be explained by the two-to-three times smaller ROIs of normal tissue compared with those of the previous study. Hence, the signal-to-noise ratio (SNR) of the CT-measured tissue enhancement curves was less pronounced in the present study. These results suggest that, at low SNR, the deconvolution algorithm used may result in underestimated CBF. Further experimental or computer simulation studies are required to understand this problem. The two-tailed *t*-test revealed no statistically significant difference between the dynamic CT and the microsphere measurements of the tissue-specific CBF CO_2 reactivity (Table 2), with values ranging from 0.7 to 0.8. Overall, these results indicate that our extended algorithm can correct for the effects of an impaired BBB such that accurate measurements of in vivo CBF and CBF CO_2 reactivities are obtained.

In the second part of this study, we compared regional CBF, CBV, and PS values in tumor, peritumor, and normal tissue obtained using our dynamic CT method (Table 3). CBF and CBV were on average 29% and 44% higher in the tumor than in the peritumor regions, respectively. Comparison of CBF and CBV between peritumor and normal tissue revealed significantly higher values in peritumor regions (28% for CBF, 38% for CBV). The very high CBF and CBV values in this VX2 carcinoma are supported by previous studies showing increased vascular proliferation in the tumor compared with normal tissue (26). The higher CBF and CBV measurements found in peritumor than those found in normal tissue support the hypothesis that feeding arterioles in the periphery of the tumor are more vasodilated than are normal vessels (28).

Evaluation of the BBB integrity (obtained by assessing PS) showed significantly higher PS values in the tumor and peritumor regions than in normal tissue (Table 3). These findings agree with the well-established fact that the capillary endothelium in neoplastic brain tissue is permeable to water, contrast molecules, and other blood plasma solutes and this permeability results in vasogenic edema in the surrounding tissue. Comparing the PS in tumor to that in normal tissue, we showed that tumor yields a value that is 20 times greater. PET studies of patients with brain tumor have also shown PS values

to be 10 to 20 times higher in the tumor than in the contralateral normal hemisphere (29, 30). A simple and accessible method that measures regional PS may prove beneficial in assessing the effects of steroids on the BBB in brain tumor (31). Such a method could also be used to evaluate the effectiveness of drugs specifically designed to modify the BBB in brain tumors in order to enhance the delivery of chemotherapeutic drugs (32).

In the third part of this investigation, we evaluated interstudy variabilities of the CT CBV and CBF measurements in brain tumors. The variability of the CBV measurements was low (7.3%) compared with findings obtained using dynamic CT methods that showed variabilities of 14% in rabbits (33) and 20% in patients (34). The variability was higher (13.2%) for the CBF than for the CBV measurements, but was lower than the 26.2% variability obtained with the standard of reference microsphere method. The microsphere-derived variability was similar to that found in normal rabbits (16). In contrast to our reported results in normal rabbits (16), variabilities in the rabbits with brain tumor were two times lower for both CT CBV (15.5% versus 7.3%) and CBF (32.5% versus 13.2%) measurements. This difference from our previous study (16) can be explained by the significantly higher SNR of the tissue enhancement curve for tumor than for normal tissue owing to leakage of contrast material in tumor (Fig 2). Because deconvolution is extremely sensitive to noise (35–37), the higher SNR of the tumor curves led to considerably less error in the estimation of CBF and CBV. As previously stated (16), a better SNR in normal tissue can be obtained by increasing the infusion rate of contrast material, by increasing the iodine concentration in the contrast material, or by increasing the tissue ROI area. Preliminary studies in normal rabbits (unpublished data) revealed an increased SNR in tissue curves by at least 50% when the infusion rate was increased from 0.3 to 1.0 mL/s while the iodine concentration and the total volume of contrast material were kept the same.

Finally, the last part of this study aimed at implementing our dynamic CT method to generate absolute CBF maps in an experimental study. These CBF maps (Fig 5) provide a clear demarcation of the high-flow tumor from the surrounding low-flow normal tissue. The CBF map during hypocapnia revealed regional changes as well as a global CBF decrease of 27% from normocapnia, underscoring the sensitivity of our CBF maps to changes in arterial CO_2. The global (ie, entire map) CBF CO_2 reactivity determined from the maps was about 1.3 mL/min/100g per mm Hg. This value is closer to the CBF CO_2 reactivity found in normal tissue (Table 2) by both the microsphere and CT methods because the maps included at least 80% normal tissue. These maps clearly enable a rapid visualization of blood flow heterogeneity in a tumor and surrounding normal tissue. Moreover, these maps accentuate the morphologic characteristics of tumor, thereby clarifying borders with normal cerebral structures better than conventional (plain) CT imaging does (Fig 5A). For clinical studies, our simple and noninvasive approach of measuring the arterial enhancement from a radial artery (38) will allow the similar creation of CBF maps with a high spatial resolution of 4 mm derived from imaging patients with brain tumors.

Some methodologic issues must be addressed regarding our dynamic CT method. First, the radiation dose of our dynamic CT technique has to be considered. The number of slices required for a dynamic CT study is about five times higher than that used for routine CT scanning of the brain (60 versus 9–17 CT slices). Nonetheless, much lower X-ray technique parameters are used in our protocol (80 kVp/80 mAs versus 120 kVp/340 mAs). Thus, the effective dose equivalent required for a dynamic CT study (~2.0 mSv) is very similar to the dose of a routine CT head scan (~1.5 mSv) (39). Furthermore, this effective dose equivalent is lower than for other blood flow measurement techniques such as PET (40) and SPECT (41) and is comparable to a *single-level* xenon CT CBF study. The mAs used to accomplish each xenon CT study are seven times higher than those used in our dynamic CT study but we have seven times more images (42). Thus, we believe that our proposed technique can reveal cerebral hemodynamics with an acceptable radiation dose.

In contrast to three-dimensional PET and SPECT perfusion studies and multilevel xenon CT, our dynamic CT method is restricted to a single anatomic level. In patients with a well-circumscribed brain tumor (eg, meningiomas, metastatic tumors), a CBF/CBV measurement at a representative slice may be sufficient for the evaluation of the nature and pathophysiologic characteristics of the disease (43). We are currently conducting studies to define the potential and limitations of single-slice CT measurements better for various clinical situations (eg, diagnosis of less sharply demarcated tumors such as gliomas). Although dynamic measurements using current CT technology at different brain levels can be obtained, this would lead to a low time resolution of contrast enhancement curves, resulting in an unacceptably low accuracy of the CBF measurements. The introduction of multislice CT scanners with the ability to scan simultaneously at different levels may overcome this limitation in the future.

Conclusion

We have experimentally validated our dynamic CT method for the absolute measurement of CBF in brain tumors as a model for tissues with a permeable BBB or blood-tissue barrier. Preliminary CBF maps derived with this method demonstrate their potential for depicting areas of different blood flow within tumors and surrounding tissue and reactivity to $PaCO_2$. The wide clinical availability of CT scanners enables the use of our dynamic CT

method to provide both anatomic and functional information with high spatial resolution for the initial diagnosis and subsequent management of patients with brain tumors.

Acknowledgments

The authors would like to thank the animal care technologist, Sarah Henderson, for her surgical preparation of the rabbits and her help in the ex vivo microsphere CBF measurements. We are also grateful to Jay Davis, MSc, for his development of the Xstatpak program used in the analysis of CT images. This project was supported by the Medical Research Council of Canada and the Canadian Anesthesia Society.

References

1. Schwartz RB. **Neuroradiology of brain tumors.** *Neurol Clin* 1995;13:723–756
2. Ricci PE, Karis JP, Heiserman JE, Fram EK, Bice AN, Drayer BP. **Differentiating recurrent tumor from radiation necrosis: time for re-evlauation of positron emission tomography?** *AJNR Am J Neuroradiol* 1998;19:407–413
3. Yoshi Y, Moritake T, Suzuki K, Fujita K, Nose T, Satou M. **Cerebral radiation necrosis with accumulation of thallium 201 on single-photon emission CT.** *AJNR Am J Neuroradiol* 1996; 17:1773–1776
4. Kline JL, Noto RB, Glantz M. **Single-photon emission CT in the evaluation of recurrent brain tumor in patients treated with gamma knife radiosurgery or conventional radiation therapy.** *AJNR Am J Neuroradiol* 1996;17:1681–1686
5. Levivier M, Becerra A, DeWitte O, Brotchi J, Goldman S. **Radiation necrosis or recurrence.** *J Neurosurg* 1996;84:148–149
6. Lammertsma AA, Wise RJS, Jones T. **In vivo measurements of regional cerebral blood flow and blood volume in patients with brain tumors using positron emission tomography.** *Acta Neurochirurgica* 1983;69:5–13
7. Bergstrom M, Collins VP, Ehrin E, et al. **Discrepancies in brain tumor extent as shown by computed tomography and positron emission tomography using [68-Ga] EDTA, [11-C] glucose, and [11-C] methionine.** *JCAT* 1983;7:1062–1066
8. Patronas NJ, Di Chiro G, Brooks RA, et al. **Work in progress: [18F] Fluorodeoxyglucose and positron emission tomography in the evaluation of radiation necrosis of the brain.** *Radiology* 1982;144:885–889
9. Patronas NJ, Di Chiro G, Kufta C, et al. **Predictions of survival in glioma patients by means of positron emission tomography.** *J Neurosurg* 1985;62:816
10. Di Chiro G, DeLa Paz RL, Brooks RA, et al. **Glucose utilization of cerebral gliomas measured by [18F] fluorodeoxyglucose and positron emission tomography.** *Neurology* 1982;32:1323–1329
11. Carvalho PA, Schwartz RB, Alexander E, et al. **Extracranial metastatic glioblastoma: Appearance on thallium-201 cloride/ technetium-99m HMPAO SPECT IMAGES.** *J Nucl Med* 1991; 32:322–324
12. Carvalho PA, Schwartz RB, Alexander EA III, et al. **Detection of recurrent gliomas with qualitative thallium-201 / technetium-99m HMPAO single-photon emission computed tomography.** *J Neurosurg* 1992;77:565–574
13. Schwartz RB, Carvalho PA, Alexander EA III, et al. **Radiation necrosis vs. high grade glioma: Differentiation by using dual-isotope SPECT with 201-Tl and 99m-Tc HMPAO.** *AJNR Am J Neuroradiol* 1991;12:1187–1192
14. Aronen HJ, Cohen MS, Belliveau JW, et al. **Ultrafast imaging of brain tumors.** *Top Magn Reson Imaging* 1993;5:14–24
15. Dean BL, Lee C, Kirsch JE, et al. **Cerebral hemodynamics and cerebral blood volume: MR assessment using gadolinium contrast agents and T1-weighted turbo-FLASH imaging.** *AJNR Am J Neuroradiol* 1992;13:39–48
16. Cenic A, Nabavi DG, Craen RA, Gelb AW, Lee T-Y. **Dynamic CT measurement of cerebral blood flow: a validation study.** *AJNR Am J Neuroradiol* 1999;20:63–73
17. Axel L. **Cerebral blood flow determination by rapid-sequence computed tomography. A theoretical analysis.** *Radiology* 1980; 137:679–686
18. Drayer BP. **Functional applications of CT of the central nervous system.** *AJNR Am J Neuroradiol* 1981;2:495–510
19. Meier P, Zierler KL. **On the theory of the indicator-dilution method for measurement of blood flow and volume.** *J Appl Physiol* 1954;6:731–744
20. St. Lawrence KS, Lee T-Y. **An adiabatic approximation to the tissue homogeneity model for water exchange in the brain: I. Theoretical derivation.** *J Cereb Blood Metab* 1998;18:1365–1377
21. Bassingthwaighte JB, Chinard FP, Crone C, Lassen NA, Perl W. **Definitions and terminology for indicator dilution methods.** In: Crone C, Lassen NA, eds. Capillary Permeability. Copenhagen: Munskgaard; 1970
22. Renkin EM. **Transport of potassium-42 from blood to tissue in isolated mammalian skeletal muscle.** *Am J Physiol* 1959;197: 1205–1210
23. Crone C. **Permeability of capillaries in various organs as determined by use of the indicator diffusion methods.** *Acta Physiol Scand* 1963;58:292–305
24. Todd MM, Weeks JB, Warner DS. **Microwave fixation for the determination of cerebral blood volume in rats.** *J Cereb Blood Flow Metab* 1993;13:328–336
25. Carson BS, Anderson JH, Grossman SA, et al. **Improved rabbit brain tumor model amenable to diagnostic radiographic procedures.** *Neurosurgery* 1982;11:603–608
26. Zagzag D, Brem S, Robert F. **Neovascularization and tumor growth in the rabbit brain. A model for experimental studies of angiogenesis and the blood-brain barrier.** *Am J Pathol* 1988;131: 361–372
27. Dewitt DS, Fatouros PP, Wist AO, et al. **Stable xenon versus radiolabeled microsphere cerebral blood flow measurements in baboons.** *Stroke* 1989;20:1716–1723
28. Endo H, Larsen B, Lassen NA. **Regional cerebral blood flow alterations remote from the site of intracranial tumors.** *J Neurosurg* 1977;46:271–281
29. Brooks DJ, Beaney RP, Lammertsma AA, et al. **Quantitative measurement of blood-brain-barrier permeability using 82-Rb and positron emission tomography.** *J Cereb Blood Flow Metab* 1984;4:535–545
30. Jarden JO. **Pathophysiological aspects of malignant brain tumors studied with positron emission tomography.** *Acta Neurologica Scandinavica* 1995;156:1–34
31. Yeung WT, Lee T-Y, Del Maestro RF, Kozak R, Bennett J, Brown T. **Effect of steroids on iopamidol blood-brain transfer constant and plasma volume in brain tumors measured with X-ray computed tomography.** *J Neuro Oncol* 1994;8:53–60
32. Fike JR, Gobbel GT, Mesiwala AH, et al. **Cerebrovascular effects of the bradykinin analog RMP-7 in normal and irradiated dog brain.** *J Neuro Oncol* 1998;37:199–215
33. Hamberg LM, Hunter GJ, Halpern EF, Hoop B, Gazelle GS, Wolf GL. **Quantitative high-resolution measurement of cerebrovascular physiology with slip-ring CT.** *AJNR Am J Neuroradiol* 1996;17:639–650
34. Steiger HJ, Aaslid R, Stooss R. **Dynamic computed tomography imaging of regional cerebral blood flow and blood volume. A clinical pilot study.** *Stroke* 1993;24:591–597
35. Gamel J, Rousseau WF, Katholi CR, Mesel E. **Pitfalls in digital computation of the impulse response of vascular beds from indicator dilution curves.** *Circ Res* 1973;32:516–523
36. Bronikowski TA, Dawson CA, Linehan JH. **Model-free deconvolution techniques for estimating vascular transport functions.** *Int J Biomed Comput* 1983;14:411–429
37. Axel L. **Tissue mean transit time from dynamic computed tomography by a simple deconvolution technique.** *Invest Radiol* 1983;18:94–99
38. Nabavi DG, Cenic A, Craen RA, Gelb AW, Lee T-Y. **CT Assessment of Cerebral Perfusion in Man. Experimental validation and initial clinical experience.** *Radiology* 1999;213:141–149
39. Huda W, Sandison GA, Lee TY. **Energy imparted and effective doses in computed tomography.** *Med Phys* 1996;23:735–741
40. Huda W, Sandison GA. **Estimates of the effective dose equivalent, H_E, in positron emission tomography studies.** *Eur J Nucl Med* 1990;17:116–120
41. Huda W, Sandison GA. **The use of the effective dose equivalents, H_E, for 99mTc labelled radiopharmaceuticals.** *Eur J Nucl Med* 1989;15:174–179
42. Johnson DW, Marks MP, Good WF, Stringer WA, Yonas H, Gur D. **Stable xenon CT cerebral blood flow imaging: rationale for and role in clinical decision making.** *AJNR Am J Neuroradiol* 1991;12:201–213
43. Palvolgyi R. **Regional cerebral blood flow in patients with intracranial tumors.** *J Neurosurg* 1969;31:149–163